Ann. Appl. Math.
doi: 10.4208/aamm

Vol. **x**, No. 1, pp. 1-28
February 202x

Specht Triangle Approximation of Large Bending Isometries

Xiang Li[1,2], and Pingbing Ming[1,2,*]

[1] *LSEC, Institute of Computational Mathematics and Scientific/Engineering Computing, AMSS, Chinese Academy of Sciences, No. 55, East Road Zhong-Guan-Cun, Beijing 100190, China*

[2] *School of Mathematical Sciences, University of Chinese Academy of Sciences, Beijing 100049, China*

Abstract. We propose a Specht triangle discretization for a geometrically nonlinear Kirchhoff plate model with large bending isometries. A combination of an adaptive time-stepping gradient flow and a Newton's method is employed to solve the ensuing nonlinear minimization problem. $\Gamma-$convergence of the Specht triangle discretization and the unconditional energy stability of the gradient flow algorithm are proved. We present several numerical examples to demonstrate that our approach significantly enhances both the computational efficiency and accuracy.

AMS subject classifications: 65N12, 65N30, 74K20

Key words: Specht triangle, plate bending, isometry constraint, adaptive time-stepping gradient flow.

1 Introduction

The geometrically nonlinear Kirchhoff plate models have drawn great attention recently because they capture the critical feature of large bending deformations of

* *Emails:* lixiang615@lsec.cc.ac.cn (X. Li), mpb@lsec.cc.ac.cn (P. B. Ming)

thin plates in modern nanotechnological applications [9, 20, 22, 27, 30]. The dimensional reduced nonlinear plate model has been proposed by Kirchhoff in 1850 [21], which is based on a curvature functional subject to a pointwise isometry constraint. Friesecke and Müller [18] have derived this model from three dimensional hyperelasticity via $\Gamma-$ convergence. Since then, extensive studies have been carried out from the perspective of modeling and numerics, such as the single layer problem [3, 13], the bilayer problem [7, 12, 14], the thermally actuated bilayer problem [6], just to mention a few. The above models all involve minimizing an energy functional with the isometry constraint. One of the numerical difficulties is the non-convexity of the model caused by the isometry constraint [5].

In this work we focus on the single layer model, and find a deformation $y:\Omega\to\mathbb{R}^3$ of a bounded Lipschitz domain $\Omega\subset\mathbb{R}^2$ by minimizing

$$E[y]=\frac{1}{2}\int_\Omega |H|^2\mathrm{d}x-\int_\Omega f(x)\cdot y(x)]\mathrm{d}x \tag{1.1}$$

subject to the isometry constraint

$$(\nabla y)^\top(\nabla y)=\mathrm{Id}_2,\ \text{a.e. in } \Omega, \tag{1.2}$$

and Dirichlet boundary condition

$$y(x)=g,\quad \nabla y=\Phi,\quad \Phi^\top\Phi=\mathrm{Id}_2\quad \text{on } \Gamma_D,$$

where $H\in L^2(\Omega;\mathbb{R}^{2\times 2})$ is the second fundamental form of the parametrized surface given by

$$H_{ij}=n\cdot\partial_i\partial_j y=(\partial_1 y\times\partial_2 y)\cdot\partial_i\partial_j y,\qquad i,j=1,2,$$

and Id_2 is the identity matrix of order 2. Γ_D is part of the boundary of D. We assume that

$$g\in H^2(\Omega;\mathbb{R}^3),\ \Phi\in H^2(\Omega;\mathbb{R}^{3\times 2}),\ f\in L^2(\Omega,\mathbb{R}^3). \tag{1.3}$$

The numerical approximation of this problem consists of two parts: discretization and minimization. A proper finite element discretization needs to take into account both high order differential operator of (1.1) and the pointwise isometry constraint. In [3, 7], the authors employed a discrete Kirchhoff triangle (DKT), which was developed in [10] for the linear bending problem. DKT element possess

the degrees of freedom of gradient at the nodes, which is convenient for imposing the constraint (1.2). The implementation of DKT element is based on the construction of a discrete gradient operator that maps the gradient to another space. Although this operator makes the proof of $\Gamma-$convergence of the discrete energy more straightforward, its numerical realization is quite complicate. Moreover, DKT is not included in the standard finite element library [13]. In addition, the quadrilateral DKT element is not suitable for the adaptive grid refinement. A discontinuous Galerkin (DG) method has been employed in [12, 13] to simulate (1.1) and (1.2). DG method has been included in many existing softwares and are more flexible in imposing the boundary conditions, while it needs a careful reconstruction of the discrete energy, and a fine-tuned penalty factor.

In the present work we turn to the nonconforming finite element method, in particular we shall exploit the Specht triangle, which is an excellent nonconforming plate bending element [31], *and passes all the patch tests and performs excellently, and is one of the best thin plate triangles with* 9 *degrees of freedom that currently available* [34, Quotation from p. 345]. The Specht triangle has been systematically studied by Shi and his collaborators in [24, 28, 29, 32]. Recently the second order Specht triangle has been designed and test in [23]. The constraint (1.2) may also be imposed on the nodes, and we prove Γ-convergence of E_h to E in $H^1(\Omega;\mathbb{R}^3)$, which shows the correctness of the energy discretization.

To ensure the energy (1.1) decreases while maintaining the constraint (1.2), a discrete H^2-gradient flow method has been designed in [3, 5, 7, 12, 13] for geometrically nonlinear Kirchhoff type models. For the single layer plate, the gradient flow exhibits two attractive properties. One is the unconditional energy stability, and the other is that the L^1 error of the constraint (1.2) is controlled by a pseudo-time step, which is independent of the number of the iteration. However, due to the first-order nature of the gradient flow method, it usually takes a large number of iteration to lower the error committed by the constraint to a reasonable threshold. To speed up the iteration, we shall exploit an adaptive time-stepping strategy developed in [16, 25, 33] for the phase filed models. Compared to [3], our method is around five times faster without loss of accuracy. We combine the H^2-gradient flow and a Newton's method to construct a global-local algorithm that improves the accuracy by around $1\sim2$ order of magnitude and results into a second order

method for examples with smooth minimizers. Similar idea has been used in [2] for simulation of the harmonic maps into sphere.

The remaining part of the paper is organized as follows. In Section 2, we use the Specht triangle to discretize the variational problem. The Γ-convergence of the discrete energy to the exact energy is proved in Section 3. In Section 4, we introduce a new method that combines a discrete adaptive time-stepping H^2-gradient flow and the Newton's method. We present numerical experiments and test the accuracy and efficiency of the method in the last section.

2 The Specht Triangle Discretization

We fix some notations firstly. The standard notations for the Sobolev spaces, the norms and semi-norms [1] will be used. The function space $L^2(\Omega)$ consists of functions that are square integrable over Ω, which is equipped with the inner product $(\cdot,\cdot)$ and the norm $\|\cdot\|_{L^2(\Omega)}$, respectively. Let $H^m(\Omega)$ be the Sobolev space of square integrable functions whose weak derivatives up to order m are also square integrable with the norm defined by $\|v\|^2_{H^m(\Omega)}:=\sum_{k=0}^m |v|^2_{H^k(\Omega)}$, where the semi-norm

$$|v|_{H^k(\Omega)}:=\sum_{|\alpha|=k}\|\partial^\alpha v\|_{L^2(\Omega)},$$

where $\alpha=(\alpha_1,\alpha_2)$ is a multi-index whose components α_i are nonnegative integers, $|\alpha|=\alpha_1+\alpha_2$ and $\partial^\alpha=\partial^{|\alpha|}/\partial x_1^{\alpha_1}\partial x_2^{\alpha_2}$. For $k\geq 0$, $H_0^k(\Omega)$ is the closure in $H^k(\Omega)$ of the space of $C^\infty(\Omega)$ functions with compact supports in Ω.

For $\mathrm{mes}\Gamma_D\neq 0$, the following Friedrich's inequality holds: for any $v\in H^1(\Omega)$ that vanishes over Γ_D, there exists C_F depending only on Γ_D and Ω such that

$$\|v\|_{L^2(\Omega)}\leq C_F\|\nabla v\|_{L^2(\Omega)}. \tag{2.1}$$

The values of Friedrichs' constant C_F may be found in [26] for simple domains such as balls, rectangles, etc.

Under the constraint (1.2), the following identity holds pointwise:

$$|H|^2=\left|D^2y\right|^2=|\Delta y|^2,$$

which was proved in [12, 13]. Hence, the energy functional $E[z]$ may be rewritten into

$$E[z]=\frac{1}{2}\int_{\Omega}\left|D^2z(x)\right|^2-\int_{\Omega}f(x)\cdot z(x)\mathrm{d}x. \tag{2.2}$$

We reshape the variational problem into

$$y=\mathrm{argmin}_{z\in\mathbb{A}}E[z], \tag{2.3}$$

where the admissible set $\mathbb{A}$ is defined by

$$\mathbb{A}:=\left\{z\in\mathbb{V}\,|\,(\nabla z)^{\top}(\nabla z)=\mathrm{Id}\text{ a.e. in }\Omega\right\}$$

with

$$\mathbb{V}:=\left\{z\in H^2(\Omega;\mathbb{R}^3)\,|\,z(x)=g,\nabla z=\Phi\text{ on }\Gamma_D\right\}.$$

2.1 The Specht triangle

Let $\mathcal{T}_h$ be a triangulation of Ω with maximum diameter h, and we assume that all the elements are shape regular in the sense of Ciarlet-Raviart [17]. We also assume that $\mathcal{T}_h$ satisfies the inverse assumption: there holds $h/h_K\leq\nu$ for $K\in\mathcal{T}_h$ and some $\nu>0$, where h_K is the diameter of the element K. We denote the set of all vertices of $\mathcal{T}_h$ by $\mathcal{V}_h$, the set of all edges of $\mathcal{T}_h$ by $\mathcal{E}_h$, and the set of all internal edges of $\mathcal{T}_h$ by $\mathcal{E}_h^{\mathrm{in}}$. Let ∇_h be a piecewise differential operator defined for any $K\in\mathcal{T}_h$ as $(\nabla_h z)|_K=(\nabla z)|_K$.

The Specht triangle is defined by a finite element triple (K,P_K,Σ_K) as:

$$\begin{cases} P_K=Z_K+b_K\mathbb{P}_1(K),\\ \Sigma_K=\{p(a_i),\partial_x p(a_i),\partial_y p(a_i),1\leq i\leq 3\},\end{cases}$$

where K is a triangle, and Z_K is the Zienkiewicz space [11] defined by

$$Z_K=\mathbb{P}_2(K)+\mathrm{Span}\left\{\lambda_i^2\lambda_j-\lambda_i\lambda_j^2\,|\,1\leq i\neq j\leq 3\right\},$$

and the element bubble function $b_K:=\lambda_1\lambda_2\lambda_3$ with $\{\lambda_i\}_{i=1}^3$ the barycentric coordinates of K.

Define the finite element space $\mathbb{X}_h$ of the Specht triangle as

$$\mathbb{X}_h:=\left\{v\in H^3(\Omega)\,|\,v|_K\in P_K,K\in\mathcal{T}_h,\ v(a),\nabla v(a)\text{ are continuous for all }a\in\mathcal{V}_h\right\}.$$

The interpolate operate Π associated with $\mathbb{X}_h$ is defined locally as $\Pi|_K=\Pi_K$ for any $v\in H^3(K)$ and

$$\Pi_K v(a)=v(a),\quad \nabla\Pi_K v(a)=\nabla v(a)\quad \text{for all } a\in\mathcal{V}_h. \tag{2.4}$$

For all $v\in H^3(\Omega)$, there holds [17]:

$$\sum_{j=0}^{2} h^j\|\nabla^j(v-\Pi v)\|_{L^2(\Omega)}\leq Ch^3\|\nabla^3 v\|_{L^2(\Omega)}. \tag{2.5}$$

For all $k=1,2,3$ and $v\in\mathbb{X}_h$, it follows from the inverse assumption that there exists C_{inv} depending on ν and k but independent of v such that

$$\|\nabla_h^k v\|_{L^2(\Omega)}\leq C_{\text{inv}}h^{-1}\|\nabla_h^{k-1}v\|_{L^2(\Omega)}. \tag{2.6}$$

2.2 Discrete energy

We approximate (2.2) by the Specht triangle. The function in $\mathbb{X}_h$ is continuous over the whole domain and its gradient is continuous at all nodes, which allows us to impose the isometry constraint (1.2) at each node. Define the discrete admissible set by

$$\mathbb{A}_h:=\left\{z\in\mathbb{V}_h\mid[(\nabla z)^\top\nabla z](a)=\text{Id for all } a\in\mathcal{V}_h\right\}$$

with

$$\mathbb{V}_h:=\left\{z\in[\mathbb{X}_h]^3\mid z(a)=g(a),\nabla z(a)=\Phi(a)\text{ for all } a\in\mathcal{V}_h\cap\Gamma_D\right\}.$$

The discrete energy minimization problem reads as

$$y_h=\text{argmin}_{z\in\mathbb{A}_h}E_h[z], \tag{2.7}$$

where

$$E_h[z]=\frac{1}{2}\int_\Omega\left|\nabla_h^2 z(x)\right|^2\mathrm{d}x-\int_\Omega f(x)\cdot z(x)\mathrm{d}x,$$

and $\int_\Omega|\nabla_h^2 z(x)|^2:=\sum\limits_{K\in\mathcal{T}_h}\int_K|\nabla^2 z|^2$ is in a piecewise manner.

Proposition 2.1. *Minimization problem* (2.7) *has a solution.*

The proof is standard, we omit it.

3 Γ-convergence of the Discrete Energy

The discrete minimization problem (2.7) is non-convex, the standard finite element error analysis fails. Instead, we prove the Γ-convergence of E_h to E in $H^1(\Omega;\mathbb{R}^3)$, which shows the correctness of our energy discretization. Following a standard Γ-convergence procedure in [15], we firstly show the compactness and equi-coercivity for any $z\in\mathbb{A}_h$, and secondly, we prove the lim-sup and lim-inf inequalities. We start with the equi-coercivity of $\{E_h\}_{h\geq 0}$.

3.1 Equi-coercivity and compactness

Lemma 3.1 (Coercivity of E_h)**.** *Let the data (f,g,Φ) satisfy (1.3). There exists a positive constant C depending on Ω,Γ_D and the triangulation, but independent of h such that for any $z\in\mathbb{A}_h$,*

$$\|z\|_{H^1(\Omega)}\leq C\left(E_h^{1/2}[z]+\|g\|_{H^2(\Omega)}+\|\Phi\|_{H^2(\Omega)}+\|f\|_{L^2(\Omega)}\right), \tag{3.1}$$

and

$$\|\nabla_h^2 z\|_{L^2(\Omega)}\leq C\left(E_h^{1/2}[z]+\|g\|_{H^2(\Omega)}+\|\Phi\|_{H^2(\Omega)}+\|f\|_{L^2(\Omega)}\right). \tag{3.2}$$

Compared to the known equi-coercivity results in the literature, we clarify the upper bound on the data and the discrete energy functional, and the constants C in (3.1) and (3.2) may also be elucidated from the proof.

Proof. For any $z\in\mathbb{A}_h$, let $\mathcal{I}_h$ be the linear Lagrange interpolation operator, note the fact that

$$\mathcal{I}_h(z-g)\in H_0^1(\Omega;\mathbb{R}^3),\quad \mathcal{I}_h(\nabla z-\Phi)\in H_0^1(\Omega;\mathbb{R}^{3\times 2}).$$

Applying the Friedrich's inequality (2.1) to $\mathcal{I}_h(z-g)$ and $\mathcal{I}_h(\nabla z-\Phi)$, we obtain

$$\begin{aligned}\|\mathcal{I}_h(z-g)\|_{L^2(\Omega)}&\leq C_F\|\nabla\mathcal{I}_h(z-g)\|_{L^2(\Omega)},\\ \|\mathcal{I}_h(\nabla z-\Phi)\|_{L^2(\Omega)}&\leq C_F\|\nabla\mathcal{I}_h(\nabla z-\Phi)\|_{L^2(\Omega)}.\end{aligned} \tag{3.3}$$

For $j=0,1$, we use the standard interpolation estimate for $\mathcal{I}_h$ and the inverse inequality (2.6) to obtain

$$\begin{aligned}\|\nabla^j(z-\mathcal{I}_h z)\|_{L^2(\Omega)}&\leq C_I h^{2-j}\|\nabla_h^2 z\|_{L^2(\Omega)},\\ \|\nabla^j(\nabla z-\mathcal{I}_h\nabla z)\|_{L^2(\Omega)}&\leq C_I h^{2-j}\|\nabla_h^3 z\|_{L^2(\Omega)}\leq C_I C_{\mathrm{inv}} h^{1-j}\|\nabla_h^2 z\|_{L^2(\Omega)}.\end{aligned} \tag{3.4}$$

Using the triangle inequality, the Friedrichs inequality (3.3) and the interpolation estimate (3.4), we obtain

$$\begin{aligned}\|\nabla z-\Phi\|_{L^2(\Omega)} &\le \|\mathcal{I}_h(\nabla z-\Phi)\|_{L^2(\Omega)}+\|(\mathrm{Id}-\mathcal{I}_h)(\nabla z-\Phi)\|_{L^2(\Omega)}\\ &\le C_F\|\nabla\mathcal{I}_h(\nabla z-\Phi)\|_{L^2(\Omega)}+C_I h\|\nabla_h(\nabla z-\Phi)\|_{L^2(\Omega)}\\ &\le C_F\|\nabla_h(\nabla z-\Phi)\|_{L^2(\Omega)}+C_F\|\nabla(\mathrm{Id}-\mathcal{I}_h)(\nabla z-\Phi)\|_{L^2(\Omega)}\\ &\quad +C_I h\big(\|\nabla_h^2 z\|_{L^2(\Omega)}+\|\nabla\Phi\|_{L^2(\Omega)}\big)\\ &\le (C_F+C_I h)\big(\|\nabla_h^2 z\|_{L^2(\Omega)}+\|\nabla\Phi\|_{L^2(\Omega)}\big)\\ &\quad +C_F\|\nabla(\mathrm{Id}-\mathcal{I}_h)\nabla z\|_{L^2(\Omega)}+C_F\|\nabla(\mathrm{Id}-\mathcal{I}_h)\Phi\|_{L^2(\Omega)}.\end{aligned}$$

Using $(3.4)_2$ with $j=1$, we obtain

$$\|\nabla(\mathrm{Id}-\mathcal{I}_h)\nabla z\|_{L^2(\Omega)}\le C_I C_{\mathrm{inv}}\|\nabla_h^2 z\|_{L^2(\Omega)},$$

and using $(3.4)_1$ with $j=1$, we obtain

$$\|\nabla(\mathrm{Id}-\mathcal{I}_h)\Phi\|_{L^2(\Omega)}\le C_I h\|\nabla^2\Phi\|_{L^2(\Omega)}.$$

A combination of the above three inequalities gives

$$\begin{aligned}\|\nabla z-\Phi\|_{L^2(\Omega)} &\le (C_F+C_I h)\big(\|\nabla_h^2 z\|_{L^2(\Omega)}+\|\nabla\Phi\|_{L^2(\Omega)}\big)\\ &\quad +C_F C_I C_{\mathrm{inv}}\|\nabla_h^2 z\|_{L^2(\Omega)}+C_F C_I h\|\nabla^2\Phi\|_{L^2(\Omega)}.\end{aligned}$$

Hence,

$$\|\nabla z\|_{L^2(\Omega)}\le A\|\nabla_h^2 z\|_{L^2(\Omega)}+(1+C_F)(1+C_I h)\|\Phi\|_{H^2(\Omega)}, \tag{3.5}$$

where $A=C_F+C_I h+C_F C_I C_{\mathrm{inv}}$.

Proceeding along the same line that leads to the above inequality, we obtain

$$\begin{aligned}\|z\|_{L^2(\Omega)} &\le C_F C_I h\|\nabla_h^2 z\|_{L^2(\Omega)}+(C_F+C_I h)\|\nabla z\|_{L^2(\Omega)}\\ &\quad +(1+C_F)(1+C_I h)\|g\|_{H^2(\Omega)}.\end{aligned}$$

A combination of the above two inequalities leads to

$$\|z\|_{L^2(\Omega)}\le \widetilde{A}\|\nabla_h^2 z\|_{L^2(\Omega)}+B\big(\|\Phi\|_{H^2(\Omega)}+\|g\|_{H^2(\Omega)}\big) \tag{3.6}$$

with

$$\widetilde{A}:=(C_F+C_Ih)A+C_FC_Ih \quad \text{and} \quad B:=(1+C_F+C_Ih)(1+C_F)(1+C_Ih).$$

It is clear that

$$E_h[z]\geq\frac{1}{2}\|\nabla_h^2 z\|_{L^2(\Omega)}^2-\|f\|_{L^2(\Omega)}\|z\|_{L^2(\Omega)}.$$

Using Young's inequality, we get

$$\begin{aligned}\|\nabla_h^2 z\|_{L^2(\Omega)}^2&\leq 2E_h[z]+2\|f\|_{L^2(\Omega)}\|z\|_{L^2(\Omega)}\\&\leq 2E_h[z]+2\|f\|_{L^2(\Omega)}\left(\widetilde{A}\|\nabla_h^2 z\|_{L^2(\Omega)}+B\left(\|\Phi\|_{H^2(\Omega)}+\|g\|_{H^2(\Omega)}\right)\right)\\&\leq 2E_h[z]+\frac{1}{2}\|\nabla_h^2 z\|_{L^2(\Omega)}^2+2\widetilde{A}^2\|f\|_{L^2(\Omega)}^2\\&\quad+2B\|f\|_{L^2(\Omega)}\left(\|\Phi\|_{H^2(\Omega)}+\|g\|_{H^2(\Omega)}\right).\end{aligned}$$

This immediately implies

$$\|\nabla_h^2 z\|_{L^2(\Omega)}\leq 2\sqrt{E_h[z]}+2\widetilde{A}\|f\|_{L^2(\Omega)}+2\sqrt{B}\|f\|_{L^2(\Omega)}^{1/2}\left(\|\Phi\|_{H^2(\Omega)}^{1/2}+\|g\|_{H^2(\Omega)}^{1/2}\right),$$

which leads to (3.2).

Substituting the above inequality into (3.5) and (3.6), we obtain

$$\begin{aligned}\|z\|_{H^1(\Omega)}&\leq 2(A+\widetilde{A})\sqrt{E_h[z]}+2(A+\widetilde{A})\widetilde{A}\|f\|_{L^2(\Omega)}\\&\quad+2(A+\widetilde{A})\sqrt{B}\|f\|_{L^2(\Omega)}^{1/2}(\|\Phi\|_{H^2(\Omega)}^{1/2}+\|g\|_{H^2(\Omega)}^{1/2})\\&\quad+2B\left(\|f\|_{L^2(\Omega)}+\|\Phi\|_{H^2(\Omega)}+\|g\|_{H^2(\Omega)}\right)\\&\leq 2(A+\widetilde{A})\sqrt{E_h[z]}\\&\quad+2\left((A+\widetilde{A})^2+B\right)\left(\|f\|_{L^2(\Omega)}+\|\Phi\|_{H^2(\Omega)}+\|g\|_{H^2(\Omega)}\right).\end{aligned}$$

This gives (3.1). □

This immediately implies

Proposition 3.1 (Equi-coercivity)**.** *Let the data* (f,g,Φ) *satisfy* (1.3)*. The sequence* $\{y_h\}_{h>0}\subset\mathbb{A}_h$ *has a uniform energy bound* $E_h[y_h]\leq\Lambda$*, where* Λ *is independent of* h*. Then the sequence* $\{y_h\}_{h>0}$ *is uniformly bounded in* $H^1(\Omega)$*, i.e.,*

$$\|y_h\|_{H^1(\Omega)}\leq C$$

with C *independent of* h*.*

The uniformly boundedness of $\{y_h\}$ in Proposition 3.1 ensures the existence of a subsequence (not relabeled) of $\{y_h\}_h$ such that

$$y_h \rightharpoonup y \ \text{ in } \ H^1(\Omega;\mathbb{R}^3) \ \textit{as} \ h\to 0,$$

for some $y\in H^1(\Omega;\mathbb{R}^3)$. We want to show that there exists $y\in\mathbb{A}\subset H^2(\Omega;\mathbb{R}^3)$ such that

$$\nabla y_h \to \nabla y \quad \text{in} \quad L^2(\Omega;\mathbb{R}^{3\times 2}).$$

Proposition 3.2. *(Compactness in $H^1(\Omega)$) Let the data (f,g,Φ) satisfy (1.3). If the sequence $\{y_h\}_{h>0}\subset\mathbb{A}_h$ has a uniform energy bound $E_h[y_h]\leq\Lambda$ for all $h>0$, where Λ is independent of h, then there exit $y\in\mathbb{A}\subset H^2(\Omega;\mathbb{R}^3)$ and a subsequence (not relabeled) of $\{y_h\}_h$ such that*

$$y_h\to y \ \textit{in} \ H^1(\Omega;\mathbb{R}^3) \ \ \textit{as} \ h\to 0.$$

Proof. It follows from Lemma 3.1 and Proposition 3.1 that $\{y_h\}_h$ and $\{\mathcal{I}_h(\nabla y_h)\}_h$ are uniform H^1 bounded, hence there exists a weakly converging subsequence of $\{y_h\}_h$ such that

$$\begin{aligned}
y_h &\to y \text{ strongly in } L^2(\Omega;\mathbb{R}^3),\\
\nabla y_h &\rightharpoonup \nabla y \text{ weekly in } L^2(\Omega;\mathbb{R}^{3\times 2}),\\
\mathcal{I}_h(\nabla y_h) &\to z \text{ strongly in } L^2(\Omega;\mathbb{R}^{3\times 2}),\\
\nabla\mathcal{I}_h(\nabla y_h) &\rightharpoonup \nabla z \text{ weekly in } L^2(\Omega;\mathbb{R}^{3\times 2\times 2}),
\end{aligned}$$

for some $y\in H^1(\Omega;\mathbb{R}^3)$ and $z\in H^1(\Omega;\mathbb{R}^{3\times 2})$ as $h\to 0$. We apply the standard interpolation estimate for $\mathcal{I}_h$ and the inverse inequality to get

$$\begin{aligned}
\|\nabla y_h - z\|_{L^2(\Omega)} &\leq \|\nabla y_h - \mathcal{I}_h(\nabla y_h)\|_{L^2(\Omega)} + \|\mathcal{I}_h(\nabla y_h) - z\|_{L^2(\Omega)}\\
&\leq Ch\|\nabla_h^2 y_h\|_{L^2(\Omega)} + \|\mathcal{I}_h(\nabla y_h) - z\|_{L^2(\Omega)},
\end{aligned}$$

which implies

$$\nabla y_h \to z \text{ in } L^2(\Omega;\mathbb{R}^{3\times 2}).$$

The uniqueness of L^2 weak limit implies $\nabla y = z$, and hence $y\in H^2(\Omega;\mathbb{R}^3)$.

Moreover, it follows from $\nabla y_h \rightharpoonup \nabla y$ and (3.2) that

$$\nabla y_h^\top \nabla y_h \rightharpoonup \nabla y^\top \nabla y \quad \text{in} \quad L^1(\Omega;\mathbb{R}^{2\times 2}).$$

It remains to prove that y is an isometry.

Note that $\mathcal{I}_h\left(\nabla y_h^\top \nabla y_h\right)=\mathrm{Id}_2$. Invoking the interpolation estimate and the inverse inequality again, we obtain

$$\begin{aligned}\|\nabla y_h^\top \nabla y_h-\mathrm{Id}_2\|_{L^1(\Omega)}&=\|\nabla y_h^\top \nabla y_h-\mathcal{I}_h(\nabla y_h^\top \nabla y_h)\|_{L^1(\Omega)}\\&\leq Ch^2\|\nabla_h^2(\nabla y_h^\top \nabla y_h)\|_{L^1(\Omega)}\\&\leq Ch^2\left(\|\nabla_h^3 y_h\|_{L^2(\Omega)}\|\nabla y_h\|_{L^2(\Omega)}+\|\nabla_h^2 y_h\|_{L^2(\Omega)}^2\right)\\&\leq Ch\left(\|\nabla_h^2 y_h\|_{L^2(\Omega)}\|\nabla y_h\|_{L^2(\Omega)}+\|\nabla_h^2 y_h\|_{L^2(\Omega)}^2\right)\\&\leq Ch,\end{aligned}\tag{3.7}$$

where we have used Lemma 3.1 in the last step.

The uniqueness of the weak limit implies that y is an isometry and this completes the proof. □

We are ready to prove Γ-convergence of E_h to E in $H^1(\Omega;\mathbb{R}^3)$. Firstly we extend the domain of discrete energy functional to $H^1(\Omega;\mathbb{R}^3)$ as follows.

$$E_h[y_h]=\begin{cases}E_h[y_h] & y_h\in\mathbb{A}_h,\\ \infty & y_h\in H^1(\Omega;\mathbb{R}^3)\backslash\mathbb{A}_h.\end{cases}\tag{3.8}$$

Theorem 3.1 (Γ-convergence)**.** *Let the data* (f,g,Φ) *satisfy* (1.3)*. The following two properties hold*

1. *Lim-inf inequality: For every sequence* $\{y_h\}_h\subset H^1(\Omega;\mathbb{R}^3)$ *converging to* y *in* $H^1(\Omega;\mathbb{R}^3)$*, we have*
$$E[y]\leq\liminf_{h\to0}E_h[y_h].$$
2. *Lim-sup inequality: For any* $y\in H^1(\Omega;\mathbb{R}^3)$*, there exits a sequence* $\{y_h\}_h$ *with* $y_h\in H^1(\Omega;\mathbb{R}^3)$ *such that* $y_h\to y$ *and*
$$\limsup_{h\to0}E_h[y_h]\leq E[y].$$

Proof. We firstly prove the lim-inf inequality. Without loss of generality, we assume that $y_h\in\mathbb{A}_h\subset H^1(\Omega;\mathbb{R}^3)$ and $E_h[y_h]\leq\Lambda$, where Λ is a positive constant independent of h. Otherwise, $\liminf_{h\to0}E_h[y_h]=+\infty$, and the lim-inf inequality holds.

Proposition 3.2 implies that $y\in\mathbb{A}\subset H^2(\Omega;\mathbb{R}^3)$. We shall show

$$\nabla_h^2 y_h \rightharpoonup \nabla^2 y \text{ weakly in } L^2(\Omega;\mathbb{R}^{3\times 2\times 2}),$$

and

$$\|\nabla^2 y\|_{L^2(\Omega)} \le \liminf_{h\to 0}\|\nabla_h^2 y_h\|_{L^2(\Omega)},$$

and

$$\begin{aligned} E[y]=\frac{1}{2}\|\nabla^2 y\|_{L^2(\Omega)}^2-\int_\Omega fy &\le \liminf_{h\to 0}\left\{\frac{1}{2}\|\nabla_h^2 y_h\|_{L^2(\Omega)}^2-\int_\Omega f y_h\right\}\\ &=\liminf_{h\to 0} E_h[y_h]. \end{aligned}$$

For any $\phi\in C_c^\infty(\Omega;\mathbb{R}^{3\times 2\times 2})$, integration by parts, we obtain

$$\begin{aligned} \int_\Omega \nabla_h^2 y_h:\phi &= \sum_{K\in\mathcal{T}_h}\int_K \nabla^2 y_h:\phi\\ &=-\sum_{K\in\mathcal{T}_h}\int_K \nabla y_h:\mathrm{div}\phi+\sum_{K\in\mathcal{T}_h}\int_{\partial K}\nabla y_h:(\phi n)\\ &=-\int_\Omega \nabla y_h:\mathrm{div}\phi+\sum_{e\in\mathcal{E}^{in}}\int_e [\![\partial_n y_h]\!]\cdot(\phi[n\otimes n])\\ &=\int_\Omega \nabla y_h:\mathrm{div}\phi+\sum_{e\in\mathcal{E}^{in}}\int_e [\![\partial_n y_h]\!]\cdot(\phi[n\otimes n]-C_e), \end{aligned}$$

for any constant vector C_e, where we have used

$$\int_e [\![\partial_n y_h]\!]=0 \qquad \text{for any edge } e$$

in the last step [28].

Denote $e=K_1\cap K_2, K=K_1\cup K_2$. Using the rescaled trace inequalities, we get

$$\begin{aligned} \left|\int_e [\![\partial_n y_h]\!]\cdot(\phi[n\otimes n]-C_e)\right| &\le \|[\![\partial_n y_h]\!]\|_{L^2(e)}\|\phi[n\otimes n]-C_e\|_{L^2(e)}\\ &\le Ch_K^{\frac{1}{2}}\|\nabla_h^2 y_h\|_{L^2(K)}(h_K^{-\frac{1}{2}}\|\phi[n\otimes n]-C_e\|_{L^2(K)}\\ &\qquad +h_K^{\frac{1}{2}}\|\nabla\phi\|_{L^2(K)})\\ &\le Ch_K\|\nabla_h^2 y_h\|_{L^2(K)}\|\nabla\phi\|_{L^2(K)}. \end{aligned}$$

Therefore, we obtain

$$\left|\sum_{e\in\mathcal{E}^{in}}\int_e[\![\partial_n y_h]\!]\cdot(\phi[n\otimes n])\right|\leq Ch\|\nabla_h^2 y_h\|_{L^2(\Omega))}\|\nabla\phi\|_{L^2(\Omega)}.$$

Taking the limit $h\to 0$, we get

$$\begin{aligned}\lim_{h\to 0}\int_\Omega\nabla_h^2 y_h:\phi&=-\lim_{h\to 0}\int_\Omega\nabla y_h:\mathrm{div}\phi+\lim_{h\to 0}\sum_{e\in\mathcal{E}^{in}}\int_e[\![\partial_n y_h]\!]\cdot(\phi[n\otimes n])\\&=-\int_\Omega\nabla y:\mathrm{div}\phi=\int_\Omega\nabla^2 y:\phi,\end{aligned}$$

i.e., $\nabla_h^2 y_h\rightharpoonup\nabla^2 y$ weakly in $L^2(\Omega;\mathbb{R}^{3\times 2\times 2})$.

Next we prove the lim-sup inequality. Without loss of generality, we assume that $y\in\mathbb{A}\subset H^2(\Omega;\mathbb{R}^3)$. The fact that smooth isometries is dense among isometries in $H^2(\Omega)^3$ [19] allows us to assume that $y\in H^3(\Omega;\mathbb{R}^3)$. Let y_h be the Specht interpolant of y, for all $a\in\mathcal{V}_h$, we get

$$[\nabla y_h^\top\nabla y_h](a)=[\nabla y^\top\nabla y](a)=\mathrm{Id}_2.$$

Hence $y_h\in\mathbb{A}_h$. Using the interpolation estimate (2.5), we obtain $y_h\to y$ in $H^2(\Omega;\mathbb{R}^3)$, and whence the convergence of the discrete energy, i.e.,

$$\lim_{h\to 0}E_h[y_h]=E[y].$$

□

Combining Proposition 3.2 and Theorem 3.1, we obtain that the cluster points of the global minimizers of E_h are global minimizers of E.

Corollary 3.1. *Let data (f,g,Φ) satisfies (1.3). Let $\{y_h\}_h$ be a sequence of almost-global minimizers of E_h, i.e.*

$$E_h[y_h]\leq\inf_{w_h\in\mathbb{A}_h}E_h[w_h]+\epsilon_h\leq C,$$

where $\epsilon_h\to 0$ as $h\to 0$ and C is a constant independent of h. Then $\{y_h\}_h$ is uniformly bounded in the H^1 norm, and every cluster point y of $\{y_h\}$ is a global minimizer of E, i.e.

$$E[y]=\inf_{w\in\mathbb{A}}E[w].$$

Moreover, there exits a subsequence of $\{y_h\}_h$(not relabeled) such that

$$y_h\to y\ \text{in}\ H^1(\Omega)\qquad\text{and}\qquad\lim_{h\to 0}E_h[y_h]=E[y].$$

4 A Combination of the Gradient Flow and Newton's method

The H^2-gradient flow algorithm developed in [3] is an efficient method to solve the problem with constraint, while the first oder convergence rate seems a hurdle for efficient implementation. To speed up the iteration, we firstly adopt the H^2-gradient flow method with an adaptive time-stepping technique, which is based on the energy variation; Such techniques appeared in the simulation of the phase field model in [25]; See also [16, 33]. Secondly, we combine the gradient flow and a Newton's method.

4.1 H^2-gradient flow

At a point $y_h \in \mathbb{X}_h^3$, we define the tangent space $\mathbb{F}_h[y_h]$ of the admissible space $\mathbb{A}_h$ by

$$\begin{aligned}\mathbb{F}_h[y_h] := \{v_h \in \mathbb{X}_h^3 : v_h|_{\Gamma_D} = 0,\ \nabla v_h|_{\Gamma_D} = 0,\\ [\nabla v_h^\top \nabla y_h](a) + [\nabla y_h^\top \nabla v_h](a) = 0 \quad \text{for all}\, a \in \mathcal{V}_h\}.\end{aligned} \tag{4.1}$$

Let $\tau > 0$ be a pseudo-time parameter, $y_h^0 \in \mathbb{A}_h$ be the initial deformation, and ϵ be the stopping threshold. Define

$$d_\tau y_h^k := \frac{1}{\tau}(y_h^{k+1} - y_h^k).$$

At $(k+1)$th step, we solve

$$y_h^{k+1} \longmapsto \min_{y_h^{k+1} \in y_h^k + \mathbb{F}_h[y_h^k]} \frac{1}{2\tau} \|\nabla_h^2 (y_h^{k+1} - y^k)\|_h^2 + E_h[y_h^{k+1}],$$

where we have included a regularized term

$$\frac{1}{2\tau} \|\nabla_h^2 (y_h^{k+1} - y^k)\|_h^2$$

to ensure the energy decay. Until the stopping criterion $\left\|\nabla_h^2 d_\tau y_h^k\right\|_{L^2(\Omega)} \le \epsilon$ is met, we find $d_\tau y_h^k \in \mathbb{F}_h[y_h^k]$ such that

$$\left(\nabla_h^2 d_\tau y_h^k, \nabla_h^2 v\right) + \left(\nabla_h^2 \left(y_h^k + \tau d_\tau y_h^k\right), \nabla_h^2 v\right) = (f, v) \qquad \text{for all} \quad v \in \mathbb{F}_h[y_h^k]. \tag{4.2}$$

We set

$$y_h^{k+1} := y_h^k + \tau d_\tau y_h^k.$$

Theorem 4.1. *Let y_h^{k+1} be the $k+1$th step solution of the gradient flow* (4.2)*, there holds*

1. *Energy decay:*

$$E_h[y_h^{k+1}]+\tau\sum_{n=0}^{k}\|\nabla_h^2 d_\tau y_h^n\|_h^2\leq E_h[y_h^0]. \tag{4.3}$$

2. *Isometry violation:*

$$\|\mathcal{I}_h([\nabla y_h^{k+1}]^T[\nabla y_h^{k+1}])-\mathrm{Id}_2\|_{L^1(\Omega)}\leq 6C_F^2(1+C_I h)^2 E_h[y_h^0]\tau. \tag{4.4}$$

Proof. Choosing $v=d_\tau y_h^k$ in (4.2), and using the elementary identity

$$a(a-b)=\frac{1}{2}(a^2-b^2)+\frac{1}{2}(a-b)^2,\qquad a,b\in\mathbb{R},$$

we get

$$E_h[y_h^{k+1}]+\frac{\tau^2+2\tau}{2}\|\nabla_h^2 d_\tau y_h^k\|_{L^2(\Omega)}^2=E_h[y_h^k],$$

which implies

$$E_h[y_h^{k+1}]+\tau\|\nabla_h^2 d_\tau y_h^k\|_h^2\leq E_h[y_h^k].$$

Using the telescoping sum, we obtain (4.3).

Note that for all $a\in\mathcal{V}_h$, there holds

$$[\nabla d_\tau y_h^k(a)]^\top[\nabla y_h^k(a)]+[\nabla y_h^k(a)]^\top[\nabla d_\tau y_h^k(a)]=0.$$

By the definition of $d_\tau y_h^k$ (4.2), we get

$$\begin{aligned}[\nabla y_h^{k+1}(a)]^\top[\nabla y_h^{k+1}(a)]&=[\nabla y_h^k(a)]^\top[\nabla y_h^k(a)]+\tau^2[\nabla d_\tau y_h^k(a)]^\top[\nabla d_\tau y_h^k(a)]\\&=\mathrm{Id}_2+\tau^2\sum_{n=0}^{k}[\nabla d_\tau y_h^n(a)]^\top[\nabla d_\tau y_h^n(a)].\end{aligned}$$

On every node $a\in\mathcal{V}_h$, we have

$$\begin{aligned}\left|[\nabla y_h^{k+1}(a)]^\top[\nabla y_h^{k+1}(a)]-\mathrm{Id}_2\right|&\leq\tau^2\sum_{n=0}^{k}\left|[\nabla d_\tau y_h^n(a)]^\top[\nabla d_\tau y_h^n(a)]\right|\\&=\tau^2\sum_{n=0}^{k}|\nabla d_\tau y_h^n(a)|^2.\end{aligned}$$

Let a,b,c be the three vertices of the element K, a direct calculation gives

$$\begin{aligned}\int_K |\mathcal{I}_h v|^2 \mathrm{d}x &= \frac{|K|}{6}\big(v^2(a)+v^2(b)+v^2(c)+v(a)v(b)+v(b)v(c)+v(c)v(a)\big)\\ &= \frac{|K|}{12}\big(v^2(a)+v^2(b)+v^2(c)+(v(a)+v(b)+v(c))^2\big)\\ &\geq \frac{|K|}{12}\big(v^2(a)+v^2(b)+v^2(c)\big).\end{aligned}$$

Hence,

$$\big\|\mathcal{I}_h\big([\nabla y_h^{k+1}]^\top[\nabla y_h^{k+1}]\big)-\mathrm{Id}_2\big\|_{L^1(\Omega)} \leq 6\tau^2\sum_{n=0}^{k}\|\mathcal{I}_h(\nabla d_\tau y_h^n)\|^2_{L^2(\Omega)}.$$

Invoking the Friedrichs' inequality (2.1) and the energy decay estimate (4.3), we obtain

$$\begin{aligned}\|\mathcal{I}_h\big([\nabla y_h^{k+1}]^\top[\nabla y_h^{k+1}]\big)-\mathrm{Id}_2\|_{L^1(\Omega)} &\leq 6C_F^2\tau^2\sum_{n=0}^{k}\|\nabla\mathcal{I}_h(\nabla d_\tau y_h^n)\|^2_{L^2(\Omega)}\\ &\leq 6C_F^2(1+C_Ih)^2\tau^2\sum_{n=0}^{k}\big\|\nabla_h^2 d_\tau y_h^n\big\|^2_{L^2(\Omega)}\\ &\leq 6C_F^2(1+C_Ih)^2\tau\big(E_h[y_h^0]-E_h[y_h^{k+1}]\big)\\ &\leq 6C_F^2(1+C_Ih)^2E_h[y_h^0]\tau.\end{aligned}$$

□

4.2 Adaptive time-stepping method

The simulation of the large bending problem needs long time computations, and the adaptive time-stepping method seems a natural choice. Theorem 4.1 implies that the H^2-gradient flow method is unconditionally stable, and the accumulation of isometry violation is related to the energy drop at each step. Therefore, we adopt a time step adaptive approach based on the energy variation to accelerate the iterations while maintaining the accuracy. Such time step adaptive strategy has been developed in [16, 25, 33] for the phase filed models. The choice of the step size τ_{k+1} is based on the variations of the energy

$$\left|\frac{E_h[y_h^k]-E_h[y_h^{k-1}]}{\tau_k}\right|^2$$

during the gradient flow iteration. In particular, if the energy changes smoothly, then the step size will be increased to accelerate the convergence. On the other hand, if the energy is changing rapidly, the step size will be decreased to maintain the isometry constraint.

At step $k+1$, we adjust the time step τ_{k+1} as

$$\tau_{k+1}=\max\left(\tau_{\min},\ \frac{\tau_{\max}}{\sqrt{1+\alpha\left|\frac{E_h[y_h^k]-E_h[y_h^{k-1}]}{\tau_k}\right|^2}}\right), \tag{4.5}$$

where the parameters $\tau_{\max}$ and $\tau_{\min}$ represent the maximum and minimum step lengths, respectively, and α is a case dependent parameter.

4.3 Newton's method

Unlike the gradient flow method, which has global convergence properties, the Newton's method is a local method, which achieves a second-order rate of convergence once a good initial point is chosen. Thus we apply Newton's method with the starting point obtained by the gradient flow method. Moreover, we find numerically that Newton's method efficiently reduces the violation error of the isometric constraints.

Three constraints of isometry $[\nabla y_h^\top \nabla y_h](a)=\mathrm{Id}_2$ on every node $a\in\mathcal{V}_h$ are

$$\begin{cases} C^{11}(a):\ \partial_1 y_h(a)\cdot\partial_1 y_h(a)-1=0,\\ C^{12}(a):\ \partial_1 y_h(a)\cdot\partial_2 y_h(a)=0,\\ C^{22}(a):\ \partial_2 y_h(a)\cdot\partial_2 y_h(a)-1=0. \end{cases}$$

We write the discrete Lagrangian as

$$\mathcal{L}(y_h,\lambda_h)=E_h(y_h)+\sum_{a\in\mathcal{V}_h}\lambda_h^1(a)C^{11}(a)+\lambda_h^2(a)C^{12}(a)+\lambda_h^3(a)C^{22}(a). \tag{4.6}$$

For every step k, we add a regularized term $\frac{1}{2\tau}\|\nabla_h^2(y_h^k-y_h^{k-1})\|_{L^2(\Omega)}^2$ of step length and apply the Newton's method as

$$\nabla^2\left(\mathcal{L}(y_h^{k-1},\lambda_h^{k-1})+\frac{1}{2\tau}\|\nabla_h^2(y_h^{k-1}-y_h^{k-1})\|_{L^2(\Omega)}^2\right)\begin{pmatrix}\tau\cdot d_\tau y_h^k\\ d_\tau\lambda_h^k\end{pmatrix}=-\nabla\mathcal{L}(y_h^{k-1},\lambda_h^{k-1}),$$

and we define

$$\begin{pmatrix} y_h^k \\ \lambda_h^k \end{pmatrix} := \begin{pmatrix} y_h^{k-1} \\ \lambda_h^{k-1} \end{pmatrix} + \begin{pmatrix} \tau \cdot d_\tau y_h^k \\ d_\tau \lambda_h^k \end{pmatrix}.$$

5 Numerical Experiments

We list the basis functions of the Specht triangle [28] for the sake of implementation. For $i=1,2,3$,

$$\begin{cases} \zeta_i = \lambda_i^2(3-2\lambda_i) + 6\sum\limits_{i\neq j} \dfrac{\nabla\lambda_i \cdot \nabla\lambda_j}{|\nabla\lambda_j|^2}\phi_j, \\ \theta_i = \lambda_i^2(\xi_j\lambda_k - \xi_k\lambda_j) + 2(\xi_j+\xi_k)b_K(\lambda_j-\lambda_k) + 3\dfrac{\nabla\lambda_i\cdot\nabla\lambda_j}{|\nabla\lambda_j|^2}\xi_j\phi_j \\ \qquad\quad -3\dfrac{\nabla\lambda_i\cdot\nabla\lambda_k}{|\nabla\lambda_k|^2}\xi_k\phi_k, \\ \omega_i = \lambda_i^2(\eta_j\lambda_k - \eta_k\lambda_j) + 2(\eta_j+\eta_k)b_K(\lambda_j-\lambda_k) + 3\dfrac{\nabla\lambda_i\cdot\nabla\lambda_j}{|\nabla\lambda_j|^2}\eta_j\phi_j \\ \qquad\quad -3\dfrac{\nabla\lambda_i\cdot\nabla\lambda_k}{|\nabla\lambda_k|^2}\eta_k\phi_k, \\ \phi_i = b_K(2\lambda_i - 1) \end{cases}$$

where $\zeta_i, \theta_i, \omega_i$ are basis functions associated with the degrees of freedom $v(a_i)$, $\partial_x v(a_i)$, $\partial_y v(a_i)$, respectively.

Define

$$I_{1h}[y_h] := \left\| \mathcal{I}_h(\nabla y_h^\top \nabla y_h) - \mathrm{Id}_2 \right\|_{L^1(\Omega)}$$

to measure the violation of the nodal isometry constraint. It follows from Theorem 4.1 that $I_{1h}[y_h]$ is of $\mathcal{O}(\tau)$. Similarly, we define

$$I_{2h}[y_h] := \left\| \nabla y_h^\top \nabla y_h - \mathrm{Id}_2 \right\|_{L^1(\Omega)},$$

as another measurement for the violation of the isometry constraint. It follows from the estimate (3.7) that $I_{2h}[y_h]$ is bounded by $\mathcal{O}(h)$. Finally, we define $\mathcal{K}_h[y_h]$ as the L^1 error of the discrete Gaussian curvature of y_h:

$$\mathcal{K}_h[y_h] := \left\| \det(-[\nabla(\mathcal{I}_h n_h)]^T [\nabla(\mathcal{I}_h y_h)]) \right\|_{L^1(\Omega)},$$

where $n_h=\partial_1 y_h\times\partial_2 y_h$ denotes the outer normal vector of the solution surface. Under isometric condition, Gauss theorema egregium implies that Guass curvature of every point of the exact solution should vanish.

The linear system of the k-th step gradient flow iteration is

$$\begin{bmatrix}(1+\tau)S & B_k^\top\\ B_k & 0\end{bmatrix}\begin{bmatrix}dY_k\\ \Lambda\end{bmatrix}=\begin{bmatrix}F-S*Y_{K-1}\\ 0\end{bmatrix}, \tag{5.1}$$

where S is the stiff matrix and B_k encodes the linearized isometry constraint.

The linear system of the k-th step of Newton's method is

$$\begin{bmatrix}(1+\tau)S+\tau S_\lambda & B_k^\top\\ B_k & 0\end{bmatrix}\begin{bmatrix}dY_k\\ \Lambda\end{bmatrix}=\begin{bmatrix}F-S*Y_{K-1}\\ 0\end{bmatrix}-F_\lambda, \tag{5.2}$$

where the two extra items F_λ and S_λ come from the exact isometric constraints in Lagrangian multiplier terms of $\mathcal{L}(y_h,\lambda_h)$. We note that the cost of each iteration of the Newton's method is similar to that of the gradient flow.

Our numerical examples are motivated by [3] and [13]. We choose $\tau_{\min}=h$, $\tau_{\max}=10h$, $\alpha=1e5$ and $\epsilon=1e-3$ unless otherwise stated. We firstly consider a simple example to test the numerical performance of our method for a relatively smooth deformation.

Example 5.1 (Rectangular plate under vertical load)**.** Let $\Omega=(0,4)\times(0,1)$. We consider the clamped boundary condition

$$y_D(x)=(x,0)^\top \text{ and } \nabla y_D(x)=[I_2,0]^\top$$

on part of the boundary $\Gamma_{\rm D}=\{0\}\times[0,1]$. We apply a constant vertical force $f(x)=(0,0,2.5\times10^{-2})^\top$ on the whole domain Ω.

In view of Table 1, we apply the gradient flow iteration on a sequence of triangulation $\mathcal{T}_2$, $\mathcal{T}_3$, $\mathcal{T}_4$ and $\mathcal{T}_5$, and take $\tau_{\min}=h$, $\tau_{\max}=10h$. The energy of the final configuration is $-1.58e-2$, while the convergence rate of both I_{1h} and I_{2h} are around 1, which is consistent with Theorem 4.1. In view of Table 5, a significant improvement in I_{1h} and I_{2h} has been observed with two extra Newton's iterations. Compared to [4], the error of I_{2h} is $1\sim2$ order of magnitude smaller, while only one sixth number of the iteration steps have been used. In view of Table 3, I_{2h}

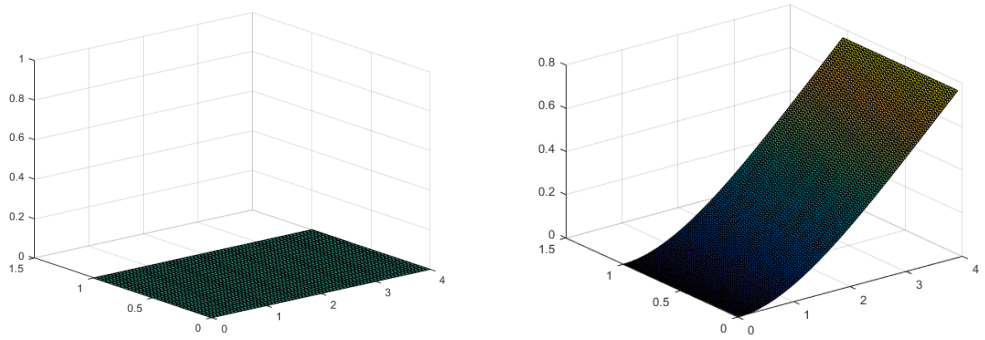

(a) Initial deformation y_h^0 (b) Deformation under vertical load.

Figure 1: The plate is clamped on one side and the vertical load is applied on the opposite side.

Table 1: The Specht triangle and H^2-gradient flow ($\tau_{\min}=h$).

No. triangles	DoFs	h	step	E_h	I_{1h}	I_{2h}	$\mathcal{K}_h$
128	765	2^{-2}	7	-1.58e-2	3.35e-2	3.35e-2	2.00e-5
512	2673	2^{-3}	11	-1.58e-2	2.12e-2	2.12e-2	4.27e-6
2048	9945	2^{-4}	18	-1.58e-2	1.26e-2	1.26e-2	8.91e-7
8192	38313	2^{-5}	32	-1.58e-2	7.09e-3	7.09e-3	1.83e-7

Table 2: Newton's method ($\tau=h$) with y_h^k from Table 1 as an initial guess.

No. triangles	DoFs	h	step	E_h	I_{1h}	I_{2h}	$\mathcal{K}_h$
128	765	2^{-2}	2	-1.58e-2	2.03e-7	3.32e-4	2.00e-5
512	2673	2^{-3}	2	-1.58e-2	1.71e-7	8.28e-5	4.27e-6
2048	9945	2^{-4}	2	-1.58e-2	1.65e-7	2.07e-5	8.93e-7
8192	38313	2^{-5}	2	-1.58e-2	6.43e-8	5.19e-6	1.81e-7

Table 3: Convergence rate: a combination of the gradient flow and the Newton's method.

h	2^{-2}	2^{-3}	2^{-4}	2^{-5}
I_{2h}	-	2.00	2.00	2.00

converges with second order, which is better than the first order rate observed in [3] and superlinear convergence observed in [13].

In what follows, we test the same example with the second order Specht triangle developed in [23] with the parameter $\alpha_1=18,\alpha_2=\alpha_3=-45$ as the spatial discretization[†]. It follows from Table 4 and Table 1 that the method with the second-order Specht triangle yields almost the same values for I_{1h} and I_{2h}. Nevertheless, it is clear in Table 4 that the accuracy is improved to certain degree for I_{1h},I_{2h} and $\mathcal{K}_h$ if we combine the Newton's method with the H^2 gradient flow method.

Table 4: The 2nd oder Specht triangle and H^2-gradient flow ($\tau_{\min}=h$).

No. triangles	DoFs	h	step	E_h	I_{1h}	I_{2h}	$\mathcal{K}_h$
128	1401	2^{-2}	7	-1.59e-2	3.35e-2	3.35e-2	9.44e-7
512	5097	2^{-3}	11	-1.58e-2	2.12e-2	2.12e-2	7.18e-7
2048	19401	2^{-4}	18	-1.58e-2	1.26e-2	1.26e-2	2.12e-7
8192	75657	2^{-5}	32	-1.58e-2	7.09e-3	7.09e-3	6.20e-8

Table 5: The 2nd order Specht triangle discretization with Newton's method: $\tau=h$ and y_h^k from Table 4 has been used as the initial guess.

No. triangles	DoFs	h	step	E_h	I_{1h}	I_{2h}	$\mathcal{K}_h$
128	1401	2^{-2}	2	-1.58e-2	1.25e-7	3.30e-4	5.01e-7
512	5907	2^{-3}	2	-1.58e-2	5.29e-8	6.41e-5	2.92e-7
2048	19401	2^{-4}	2	-1.58e-2	1.56e-8	1.20e-5	8.93e-7
8192	75657	2^{-5}	2	-1.58e-2	4.50e-9	2.60e-6	7.33e-8

Example 5.2 (Square plate under vertical load)**.** Let $\Omega=(0,4)\times(0,4)$. We consider the clamped boundary condition

$$y_D(x)=(x,0)^\top \text{ and } \nabla y_D(x)=[I_2,0]^\top$$

on part of the boundary $\Gamma_{\rm D}=\{0\}\times[0,4]\cup[0,4]\times\{0\}$. We then apply a constant vertical force $f(x)=(0,0,2.5\times10^{-2})^\top$ on the whole domain Ω.

[†]There are many choices of the second order Specht triangle in [23]. We take the one with the best numerical performance.

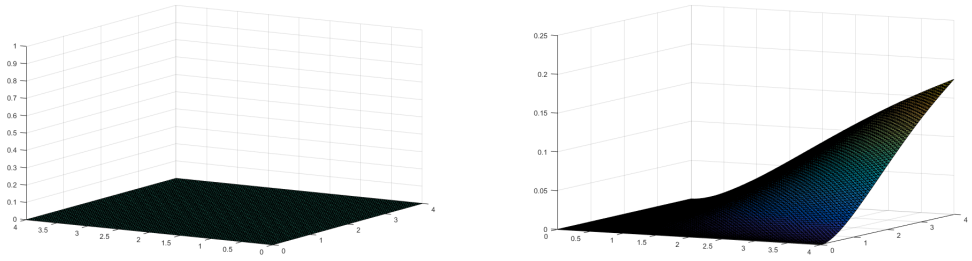

(a) Initial deformation y_h^0.

(b) Deformation under the vertical load over the triangulation $\mathcal{T}_4$.

Figure 2: vertical load

Table 6: The Specht triangle and H^2-gradient flow.

No. triangles	DoFs	h	step	E_h	I_{1h}	I_{2h}	$\mathcal{K}_h$
512	2304	2^{-2}	5	-1.01e-2	9.61e-3	1.20e-2	3.37e-3
2048	9216	2^{-3}	7	-9.69e-3	5.97e-3	8.76e-3	2.87e-3
8192	36,864	2^{-4}	10	-8.69e-3	3.01e-3	5.38e-3	2.05e-3
32,768	147,456	2^{-5}	16	-7.13e-3	1.27e-3	2.79e-3	1.27e-3

Table 7: Comparison of DKT [3], DG method [13] and our method (without Newton's method) of the same example on the triangulation $\mathcal{T}_5$.

Methods	DoFs	h	step	E_h	I_{2h}	$\mathcal{K}_h$
DKT	147,456	2^{-5}	130	-7.67e-3	3.03e-3	1.47e-3
DG	491,520	2^{-5}	140	-3.30e-3	2.28e-4	*
ours	147,456	2^{-5}	16	-7.13e-3	2.79e-3	1.27e-3

Table 8: Newton method with y_h^k from Table 6 as the initial guess.

No. triangles	DoFs	h	step	E_h	I_{1h}	I_{2h}	$\mathcal{K}_h$
512	2304	2^{-2}	2	-9.95e-3	5.91e-8	8.04e-3	3.30e-3
2048	9216	2^{-3}	2	-9.46e-3	3.03e-8	6.58e-3	2.76e-3
8192	36,864	2^{-4}	2	-8.40e-3	1.29e-8	4.39e-3	1.96e-3
32768	147,456	2^{-5}	2	-6.89e-3	3.66e-9	2.42e-3	1.22e-3

Table 9: Convergence rate: a combination of the gradient flows and Newton's method.

h	2^{-2}	2^{-3}	2^{-4}	2^{-5}
I_{2h}	-	0.29	0.58	0.86

In view of Table 6, we apply the H^2-gradient flow algorithm with adaptive time-stepping to a sequence of triangulations $\mathcal{T}_2$, $\mathcal{T}_3$, $\mathcal{T}_4$ and $\mathcal{T}_5$. The convergence rates of both I_{1h} and I_{2h} are still around 1, and the iteration steps of our method are robust to the variation of the mesh size.

In view of Table 7, compared to [3] and [13], our adaptive strategy significantly reduces the number of the iteration. In particular on the triangulation $\mathcal{T}_5$, the DKT element in [3] required 130 iteration steps, and the DG method in [13] required 140 iteration steps, while our method achieves the same accuracy as [3] with only 16 iteration steps.

In view of Table 8 and Table 9, Newton's method is effective in reducing I_{1h}. However, I_{2h} remains at a similar magnitude and the convergence rate is only around 1. This could be attributed to the way the isometry constraints (1.2) is imposed, as well as the nature of the example, which is highly prone to the violation of the isometry constraints.

Another attractive example is the bulking of a plate.

Example 5.3 (Buckling: compress a strip)**.** Let $\Omega=(-2,2)\times(0,1)$. We impose the compressive boundary conditions

$$y_D(x)=(x_1+1.4,x_2,0)^\top \quad \text{and} \quad \nabla y_D(x)=[\mathrm{Id}_2,0]^\top$$

on the two sides $\Gamma_{\mathrm{D}}=\{-2,2\}\times[0,1]$, and we apply constant verical force $f(x)=(0,0,1.0\times10^{-5})^\top$ on the whole domain Ω.

We choose the initial deformation y_h^0 as

$$y_h^0(x)=\begin{cases}(x_1+1.4,x_2,0), & -2\le x_1\le -1.4,\\ (0,x_2,x_1+1.4), & -1.4\le x_1\le 0,\\ (0,x_2,-x_1+1.4), & 0\le x_1\le 1.4,\\ (x_1-1.4,x_2,0), & 1.4\le x_1\le 2,\end{cases}$$

and set

$$\Phi = \begin{pmatrix} 1 & 0 \\ 0 & 1 \\ 0 & 0 \end{pmatrix}.$$

We plot the initial guess and the deformed state in Figure 5.

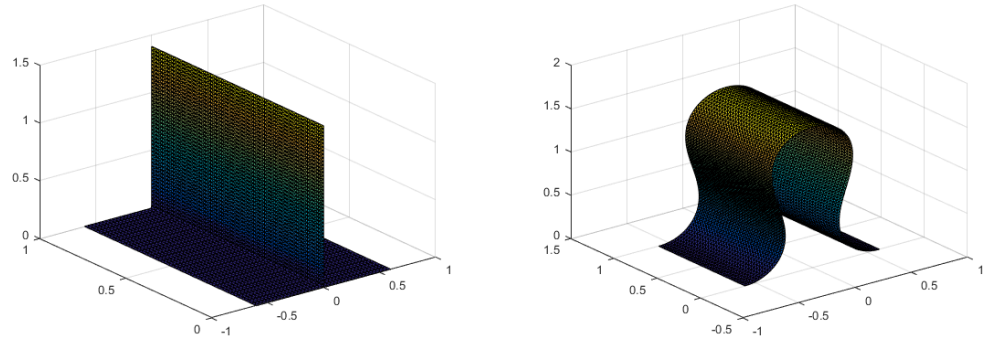

(a) Initial guess y_h^0. (b) Buckling.

Figure 3: Buckling

Note that the initial guess is incompatible in the sense that $\|\nabla y_h^0 - \Phi\|_{L^2(\Omega)} \neq 0$, which yields a relatively high initial energy $E[y_h^0]$, we hence adjust the parameters of the adaptive time-stepping to $\tau_{\max} = 100\tau_{\min}$ and $\alpha = 1e-4$.

By Figure 3, a bulking deformation occurs, and we display the results in Table 10, and it seems challenging to maintain I_{1h} and I_{2h} in this example.

Table 10: Specht triangle, H^2-gradient flow: Number of triangles, degrees of freedom, number of the gradient flow iteration, energy, L_1-norm of the violation of isometry, L_1-norm of the discrete Gauss curvature.

No. triangles	DoFs	h	step	E_h	I_{1h}	I_{2h}	$\mathcal{K}_h$
128	765	2^{-2}	22	56.35	35.04	33.88	1.83e-1
512	2304	2^{-3}	14	23.04	12.51	12.39	3.67e-2
2048	9216	2^{-4}	30	9.16	0.62	0.61	5.69e-3
8192	36,864	2^{-5}	75	9.94	1.35	1.34	4.72e-3

In Table 11, we fix the mesh size as $h = 2^{-5}$ and take $\tau_{\min}$ to be $h^{1/2}$, h, $h^{3/2}$, respectively. It takes 367 steps to reduce I_{2h} to $9.82e-2$, whereas the author in [3]

required 2,457 steps to reduce I_{2h} to $6.91e{-}2$ with $\tau = h^{3/2}$. Next we use results y_h^k

Table 11: H^2- gradient flow: $h = 2^{-5}$, pseudo-time step, the number of the iteration step, L^1-norm of the violation of the isometry, energy.

τ	step	I_{1h}	I_{2h}	E_h	$\mathcal{K}_h$
$h^{1/2}$	18	1.29	1.29	10.02	5.25e-2
h	71	1.35	1.34	9.94	4.75e-3
$h^{3/2}$	367	9.82e-2	9.64e-2	8.66	2.71e-4

from Table 10 as an initial guess of Newton's method, and still take $\epsilon_{stop} < 1e{-}3$. Table 12 shows that I_{1h} can be reduced to $1e{-}8$ and I_{2h} to $1e{-}3$ after several additional Newton's iteration steps.

Table 12: The Specht triangle and the Newton's method with y_h^k from Table 10 as an initial guess.

No. triangles	DoFs	h	step	E_h	I_{1h}	I_{2h}	$\mathcal{K}_h$
128	765	2^{-2}	46	8.08	1.61e-8	1.96e-1	7.16e-3
512	2304	2^{-3}	45	8.45	7.74e-8	5.25e-2	1.38e-3
2048	9216	2^{-4}	19	8.55	3.22e-8	1.34e-2	2.17e-4
8192	36,864	2^{-5}	37	8.57	3.56e-8	3.36e-3	1.20e-4

Acknowledgments

This work is supported by National Natural Science Foundation of China through Grant No. 11971467.

References

[1] R. Adams and J. Fournier, *Sobolev Spaces*, 2nd eds. ed., Academic Press, Boston.

[2] S. Bartels, *Combination of global and local approximation schemes for harmonic maps into spheres*, J. Comput. Math. (2009), 170–183.

[3] ———, *Approximation of large bending isometries with discrete Kirchhoff triangles*, SIAM J. Numer. Anal. **51** (2013), no. 1, 516–525.

[4] ———, *Finite element approximation of large bending isometries*, Numer. Math. **124** (2013), no. 3, 415–440.

[5] ———, *Finite element simulation of nonlinear bending models for thin elastic rods and plates*, Geometric partial differential equations. Part I, Handb. Numer. Anal., vol. 21, Elsevier/North-Holland, Amsterdam, [2020] ©2020, pp. 221–273. MR 4378428

[6] S. Bartels, A. Bonito, A. H. Muliana, and R. H. Nochetto, *Modeling and simulation of thermally actuated bilayer plates*, J. Comput. Phys. **354** (2018), 512–528.

[7] S. Bartels, A. Bonito, and R. H. Nochetto, *Bilayer plates: model reduction, Γ-convergent finite element approximation, and discrete gradient flow*, Comm. Pure Appl. Math. **70** (2017), no. 3, 547–589.

[8] S. Bartels and C. Palus, *Stable gradient flow discretizations for simulating bilayer plate bending with isometry and obstacle constraints*, arXiv preprint arXiv:2004.00341 (2020).

[9] N. Bassik, B. T. Abebe, K. E. Laflin, and D. H. Gracias, *Photolithographically patterned smart hydrogel based bilayer actuators*, Polymer **51** (2010), no. 26, 6093–6098.

[10] J.-L. Batoz, K.-J. Bathe, and L.-W. Ho, *A study of three-node triangular plate bending elements*, Int. J. Numer. Meth. Eng. **15** (1980), no. 12, 1771–1812.

[11] G. P. Bazeley, Y. K. Cheung, B. M. Irons, and O. C. Zienkiewicz, *Triangular elements in bending-conforming and non-conforming solutions*, In Proc. 1st Conf. Matrix Methods in Structure Mechanics, Volume AFFdL-TR-66-80, Wright Patterson Air Force Bases, Ohio, pages 547-576, 1966.

[12] A. Bonito, R. H. Nochetto, and D. Ntogkas, *Discontinuous galerkin approach to large bending deformation of a bilayer plate with isometry constraint*, J. Comput. Phys. **423** (2020), 109785.

[13] ———, *Dg approach to large bending plate deformations with isometry constraint*, Math. Mod. Meth. Appl. Sci. **31** (2021), no. 01, 133–175.

[14] A. Bonito, R. H. Nochetto, and S. Yang, *Γ-convergent ldg method for large bending deformations of bilayer plates*, arXiv preprint arXiv:2301.03151 (2023).

[15] A. Braides, *Local minimization, variational evolution and Γ-convergence*, vol. 2094, Springer, 2014, Lecture Notes in Mathematics.

[16] Y. Chen and J. Shen, *Efficient, adaptive energy stable schemes for the incompressible Cahn–Hilliard Navier–Stokes phase-field models*, J. Comput. Phys. **308** (2016), 40–56.

[17] P.G. Ciarlet, *The Finite Element Method for Elliptic Problems*, North-Holland, Am-

sterdam, 1978.

[18] G. Friesecke, R. D. James, and S. Müller , *A theorem on geometric rigidity and the derivation of nonlinear plate theory from three-dimensional elasticity*, Comm. Pure Appl. Math. **55** (2002), no. 11, 1461–1506.

[19] P. Hornung, *Approximation of flat $W^{2,2}$ isometric immersions by smooth ones*, Arch. Ration. Mech. Anal. **199** (2011), 1015–1067.

[20] E. Jager, E. Smela, and O. Inganas, *Microfabricating conjugated polymer actuators*, Science **290** (2000), no. 5496, 1540–1545.

[21] G. Kirchhoff, *Über das Gleichgewicht und die Bewegung einer elastischen Scheibe.*, J. Reine Angew. Math. **40** (1850), 51–88.

[22] J.-N. Kuo, G.-B. Lee, W.-F. Pan, and H.-H. Lee, *Shape and thermal effects of metal films on stress-induced bending of micromachined bilayer cantilever*, Japanese J. Appl. Phys. **44** (2005), no. 5R, 3180.

[23] H.L. Li, P.B. Ming, and Z.-C. Shi, *The quadratic Specht triangle*, J. Comput. Math. **38** (2020), no. 1, 103–124.

[24] H.L. Li, P.B. Ming, and H.Y. Wang, *H^2-korn's inequality and the nonconforming elements for the strain gradient elastic model*, J. Sci. Comput. **88** (2021), 78.

[25] Z. H. Qiao, Z. R. Zhang, and T. Tang, *An adaptive time-stepping strategy for the molecular beam epitaxy models*, SIAM J. Sci. Comput. **33** (2011), no. 3, 1395–1414.

[26] S.I. Repin, *Computable majorants of constants in the Poincaré and Friedrichs inequalities*, J. Math. Sci. **186** (2012), 307–321, Translated from Problems in Mathematical Analysis, 66, August 2012, pp. 153–165.

[27] O. G. Schmidt and K. Eberl, *Thin solid films roll up into nanotubes*, Nature **410** (2001), no. 6825, 168–168.

[28] Z.-C. Shi and S.C. Chen, *An analysis of a nine-parameter plate element of Specht*, Math. Numer. Sinica **3** (1989), 312–318.

[29] Z.-C. Shi and J.C. Wang, *A note on equivalence of some triangular plate elements*, Math. Numer. Sinica **21** (1999), 39–44.

[30] E. Smela and and I. Lundström O. Inganäs, *Controlled folding of micrometer-size structures*, Science **268** (1995), no. 5218, 1735–1738.

[31] B. Specht, *Modified shape functions for the three-node plate bending element passing the patch test*, Int. J. Numer. Meth. Eng. **26** (1988), 705–715.

[32] M. Wang, Z.-C. Shi, and J. Xu, *A new class of Zienkiewicz-type non-conforming element in any dimensions*, Numer. Math. **106** (2007), 135–147.

[33] Z. R. Zhang, Y. Ma, and Z. H. Qiao, *An adaptive time-stepping strategy for solving*

the phase field crystal model, J. Comput. Phys. **249** (2013), 204–215.

[34] O. C. Zienkiewicz, R. L. Taylor, and D. Fox, *The Finite Element Method: Solid Mechanics*, vol. 2, Butterworth-heinemann, 2000.